

## Article

# High-Temperature Interactions of Silicon-Aluminum Oxynitrides (Sialons) with Sodium Fluoride

Nailya S. Akhmadullina \*, Vladimir P. Sirotnkin, Nikolay A. Ovsyannikov, Anton S. Lysenkov  and Yury F. Kargin

A.A. Baikov Institute of Metallurgy and Material Science, Russian Academy of Sciences, Leninsky Avenue 49, 119334 Moscow, Russia

\* Correspondence: nakhmadullina@mail.ru; Tel.: +7-919-109-03-32

**Abstract:** The high-temperature interactions of  $\beta$ -SiAlONs with sodium fluoride NaF at 1650 °C under a nitrogen atmosphere are described in this paper. It was found that in case of Si<sub>5</sub>AlON<sub>7</sub> the formation of phases enriched with aluminum occurred, including Si<sub>4</sub>Al<sub>2</sub>O<sub>2</sub>N<sub>6</sub> at an NaF loading of 0.5 wt.% and Si<sub>4</sub>Al<sub>2</sub>O<sub>2</sub>N<sub>6</sub> and Si<sub>3.1</sub>Al<sub>2.9</sub>O<sub>2.9</sub>N<sub>5.1</sub> at an NaF loading of 2.0 wt.%, although Si<sub>5</sub>AlON<sub>7</sub> still was a major phase. For Si<sub>4</sub>Al<sub>2</sub>O<sub>2</sub>N<sub>6</sub>, a kind of disproportionation was observed, and Si<sub>5</sub>AlON<sub>7</sub> formed together with Si<sub>3</sub>Al<sub>3</sub>O<sub>3</sub>N<sub>5</sub> and Si<sub>3.1</sub>Al<sub>2.9</sub>O<sub>2.9</sub>N<sub>5.1</sub>. Moreover, the initial phase Si<sub>4</sub>Al<sub>2</sub>O<sub>2</sub>N<sub>6</sub> was not identified at all, while Si<sub>5</sub>AlON<sub>7</sub> was found to be a major phase at an NaF loading of 0.5 wt.% and Si<sub>3.1</sub>Al<sub>2.9</sub>O<sub>2.9</sub>N<sub>5.1</sub> prevailed at an NaF loading of 2.0 wt.%. All the samples showed a high degree of densification when studied with scanning electronic microscopy.



**Citation:** Akhmadullina, N.S.; Sirotnkin, V.P.; Ovsyannikov, N.A.; Lysenkov, A.S.; Kargin, Y.F. High-Temperature Interactions of Silicon-Aluminum Oxynitrides (Sialons) with Sodium Fluoride. *Inorganics* **2022**, *10*, 140. <https://doi.org/10.3390/inorganics10090140>

Academic Editors: Duncan H. Gregory, Torben R. Jensen, Claudio Pettinari, Vladimir Arion, Wolfgang Linert and Richard Dronskowski

Received: 5 August 2022

Accepted: 13 September 2022

Published: 16 September 2022

**Publisher's Note:** MDPI stays neutral with regard to jurisdictional claims in published maps and institutional affiliations.



**Copyright:** © 2022 by the authors. Licensee MDPI, Basel, Switzerland. This article is an open access article distributed under the terms and conditions of the Creative Commons Attribution (CC BY) license (<https://creativecommons.org/licenses/by/4.0/>).

**Keywords:** sialon; sodium fluoride; high-temperature treatment; phase transformation

## 1. Introduction

Nitride ceramics show high thermal, chemical, and mechanical stability, which make them widely used materials in the mechanical engineering, aerospace, chemical, and medical industries [1–7]. Silicon-aluminum oxynitrides (SiAlONs or sialons) are used to produce parts of automotive engines, heavy-loaded bearings, blades of gas turbines, etc., due to their effective densification, high sintering properties and easy processing [1,8–13]. At the same time, the synthesis of SiAlONs of a given composition and properties is still quite a challenge. SiAlONs are solid solutions formed because of the substitution of silicon and nitrogen in silicon nitride by aluminum and oxygen in a wide range of concentrations [10]. Six general types of SiAlONs are known today, including  $\alpha$ -,  $\beta$ -, O'-, X-, R- and H-SiAlONs.  $\alpha$ -SiAlONs are derivatives of  $\alpha$ -Si<sub>3</sub>N<sub>4</sub>, and they can be described with the general formula Me<sub>m/z</sub>Si<sub>12-m-n</sub>Al<sub>m+n</sub>O<sub>n</sub>N<sub>16-n</sub>, where Me is a metal with a valency  $z$  [14,15].  $\alpha$ -SiAlONs are difficult to prepare, since the initial  $\alpha$ -Si<sub>3</sub>N<sub>4</sub> structure is unstable under typical synthesis conditions and can only be stabilized in the presence of Me ions. O'-SiAlONs are isostructural to silicon oxynitride Si<sub>2</sub>N<sub>2</sub>O, whose structure consists of the layers formed by Si<sub>3</sub>N<sub>4</sub> rings and linked by Si-O-Si bonds. In O'-SiAlONs, Al and O replace some of the Si and N atoms; therefore, the general formula is Si<sub>2-z</sub>Al<sub>z</sub>N<sub>2-z</sub>O<sub>1+z</sub> with  $z < 0.4$  [16]. X-SiAlON is a Si<sub>12</sub>Al<sub>18</sub>O<sub>39</sub>N<sub>8</sub> compound with a narrow homogeneity region [17,18]. X-SiAlON shows a triclinic structure, and the cell ideally contains six Si<sub>3</sub>Al<sub>6</sub>O<sub>12</sub>N<sub>2</sub> units. The structure in general consists of alternating chains of octahedra and tetrahedra linked in layers. The layers are packed parallel to each other and connected by a network of tetrahedra, some elements of which resemble the elements of Si<sub>6</sub>N<sub>8</sub> cells in the  $\beta$ -Si<sub>3</sub>N<sub>4</sub> structure. R- and H-SiAlONs are solid solutions of the composition  $z$ AlN·SiO<sub>2</sub>. The solutions are ordered polytypes with a layered structure described by the Ramsdell symbols 8H ( $z = 3$ ), 15R ( $z = 4$ ), 12H ( $z = 5$ ), 21R ( $z = 6$ ), 27R ( $z = 8$ ), and 2H<sup>δ</sup> [8,19–21].

$\beta$ -SiAlONs are derivatives of  $\beta$ -Si<sub>3</sub>N<sub>4</sub> of the general formula Si<sub>6-z</sub>Al<sub>z</sub>O<sub>z</sub>N<sub>8-z</sub>,  $z = 0 \div 4.2$  [14,22–24].  $\beta$ -Si<sub>3</sub>N<sub>4</sub> is the most stable form of silicon nitride, so  $\beta$ -SiAlONs can

be prepared via the direct reaction of  $\text{Si}_3\text{N}_4$ ,  $\text{Al}_2\text{O}_3$ ,  $\text{SiO}_2$ , and  $\text{AlN}$  with no additional metal ions. Due to the wide range of properties and easier preparation compared to other types,  $\beta$ -SiAlONs may be considered as the most prospective SiAlON ceramics. At the same time, there are still some issues which need to be addressed to extend their application area.

The first issue is a high temperature required for synthesis. That is a result of the rather low diffusion rate, which becomes noticeable only at a temperature above 1700 °C, when partial decomposition of  $\text{Si}_3\text{N}_4$  can already occur. Therefore, new synthetic approaches are currently being actively developed using sintering additives, which facilitate the formation of a liquid phase and make it possible to reduce the sintering temperature under pressure or without it [25]. Densification and sintering of various types of  $\text{Si}_3\text{N}_4$  and SiAlONs can be achieved using oxide additives such as  $\text{Y}_2\text{O}_3$ ,  $\text{Al}_2\text{O}_3$ , and  $\text{MgO}$ , as well as fluorides, primarily  $\text{MgF}_2$  and  $\text{CaF}_2$  [26,27]. At the same time, alkali metal fluorides (e.g.,  $\text{NaF}$ ,  $\text{LiF}$ ) are more often used for the stabilization of  $\alpha$ -SiAlON [28,29].

Furthermore, the fabrication of transparent ceramics based on SiAlONs is also still quite a challenge [30]. Most transparent ceramic materials are characterized by a cubic structure; their transparency does not depend on the layer thickness. Although SiAlONs have a hexagonal structure, which causes birefringence, and their optical properties are noticeably worse than those of ceramics with a cubic structure, the optical properties can be significantly improved by achieving a suitable grain size and structure, as was shown, for example, for polycrystalline alumina [31]. Fluorine-based additives can also be helpful in this case [32,33].

By decreasing the glass transition temperature and facilitating glass formation in SiAlON systems, on the other hand, fluorides can be also considered as corrosive media for oxynitride ceramics [34]. For  $\beta$ -SiAlONs, incorporation of a significant amount of fluorine may cause a decrease in Vicker's hardness, for example [35]. So, the following conclusions can be made from the listed examples:

1. Fluorides of light metals (e.g., Li, Na, Ca, Mg, and Al) can be effective auxiliary additives for the fabrication of SiAlONs including glasses;
2. Some possible negative side effects have to be kept in mind when fluorides are used;
3. An excess of fluorine in the composition of oxynitride may be undesirable considering some of the mechanical properties;
4. Fluorides are corrosive media for oxynitride ceramics and may induce their decomposition and changes in the phase compositions.

Usually, fluorides are used as auxiliary additives during the synthesis process. For example, Hampshire and co-workers studied pressureless preparation of  $\beta$ -SiAlON ceramic compositions using  $\text{MgO}/\text{Y}_2\text{O}_3$  and  $\text{MgF}_2/\text{Y}_2\text{O}_3$  additive systems [36]. They noted that the produced samples showed a density up to 100% compared to the theoretical values. In addition, at lower temperatures,  $\text{MgF}_2$ -doped  $\beta$ -SiAlON ceramics have a higher hardness than  $\beta$ -SiAlON doped with  $\text{MgO}$ . It should be mentioned that only  $\beta$ -SiAlON with  $z = 1$  was studied and  $\text{MgF}_2$  was used together with  $\text{Y}_2\text{O}_3$ , so it is not possible to differentiate the effects from both additives.

To the best of our knowledge, there is no data for high-temperature  $\beta$ -SiAlON behavior in the presence of the fluorides except for studies of corrosion in surface layers [34,37]. So, the goal of the presented study was to investigate the effect of sodium fluoride  $\text{NaF}$  as a sintering additive for prefabricated  $\beta$ -SiAlONs with  $z = 1$  and 2 on their composition and structure.

## 2. Results and Discussion

### 2.1. Starting Materials

The starting materials were powders of  $\beta$ -SiAlONs, which were received from "Plas-motherm" LLC and characterized with X-ray diffraction analysis (samples **SiAlON-1** and **SiAlON-2**). XRD patterns are given in Figure 1. According to the collected data, both samples were  $\beta$ -SiAlONs, the sample **SiAlON-1** was  $\text{Si}_5\text{AlON}_7$  and the sample **SiAlON-2** was  $\text{Si}_4\text{Al}_2\text{O}_2\text{N}_6$ . The **SiAlON-1** sample showed a set of peaks at 23.34, 27.00, 33.39, 35.94,

38.70, 41.10, 47.67, 49.71, 51.84, 57.57, 59.40, 61.05, 63.30, 64.50, 69.69, 71.22, 73.02, and 74.85°, which are characteristic for  $\text{Si}_5\text{AlON}_7$  (Figure 1a, ICDD 00-048-1615). The **SiAlON-2** sample had a similar XRD pattern, however, all the peaks were shifted giving a picture typical for a  $\text{Si}_4\text{Al}_2\text{O}_2\text{N}_6$  phase. The peaks were found at 23.28, 26.94, 33.33, 35.88, 38.61, 41.01, 47.58, 49.62, 51.78, 57.48, 59.31, 60.96, 63.15, 64.44, 69.66, 71.13, 72.93, and 74.82° (Figure 1c, ICDD 01-076-0599). The presence of peaks at ~24.5, 29.7, 30.1, 32.0, 39.8, 39.5, and 39.7° in both the samples indicated an impurity of X-SiAlON  $\text{Si}_2\text{Al}_3\text{O}_7\text{N}$  (Figure 1b,d, ICDD 00-035-0023) with a content below 3 v/v %. Thus, the samples were homogenous in composition and structure, which was also confirmed by scanning electron microscopy combined with energy-dispersive X-ray spectroscopy (Figure 2). As one can see, the **SiAlON-1** and **SiAlON-2** samples mainly consisted of uniform particles up to 2  $\mu\text{m}$  in size with an irregular shape, which were highly likely agglomerates of smaller particles. In addition, a few rods and plates up to 5  $\mu\text{m}$  in size could be identified in all the images, however, their composition was close to the average composition of the samples, so they did not present impurity phases mentioned above. The elements constituting the samples (Si, Al, O, and N) were evenly distributed in the volume of the samples, and the element contents corresponded to the expected compositions, considering the accuracy of determination, as well as the excess oxygen content in the surface layer (Table 1).

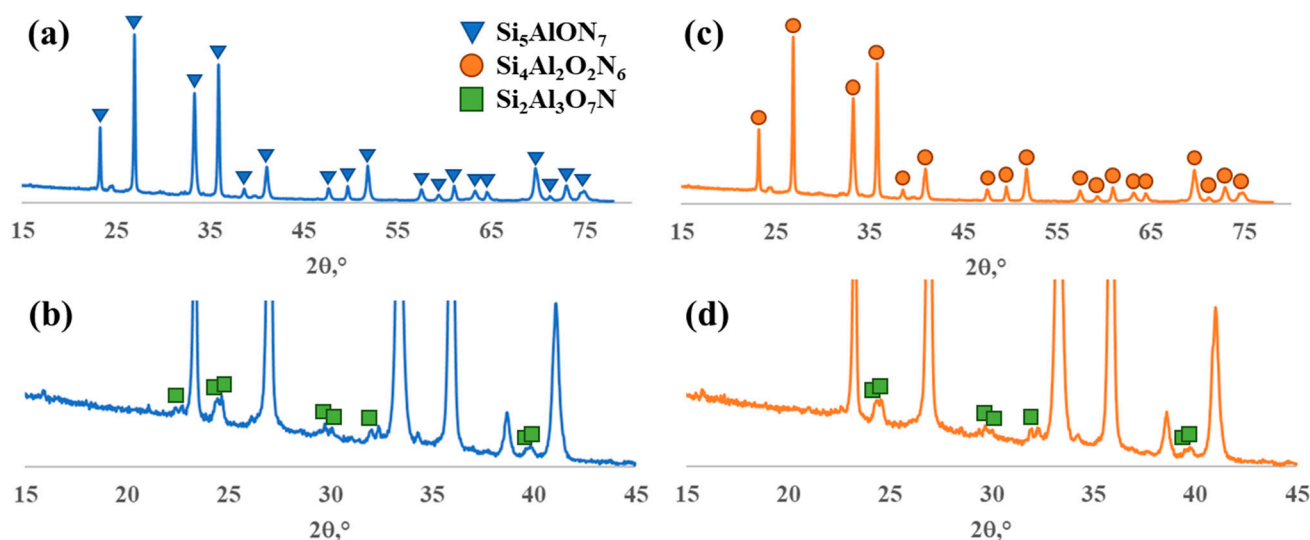


**Figure 1.** XRD-pattern of the samples **SiAlON-1** (a,b) and **SiAlON-2** (c,d).

**Table 1.** Average content of elements in the samples **SiAlON-1** and **SiAlON-2** according to energy dispersive X-ray spectroscopy.

Sample	Si, at. %	Al, at. %	O, at. %	N, at. %
<b>SiAlON-1</b> ( $\text{Si}_5\text{AlON}_7$ )	35.1	5.6	9.5	49.8
Theoretical composition	50.0	7.15	7.15	35.7
Generalized formula		$\text{Si}_5\text{Al}_{0.8}\text{O}_{1.9}\text{N}_{6.4}$		
<b>SiAlON-2</b> ( $\text{Si}_4\text{Al}_2\text{O}_2\text{N}_6$ )	30.6	14.7	20.4	34.3
Theoretical composition	28.6	14.3	14.3	42.8
Generalized formula		$\text{Si}_4\text{Al}_{1.9}\text{O}_{2.7}\text{N}_{4.5}$		

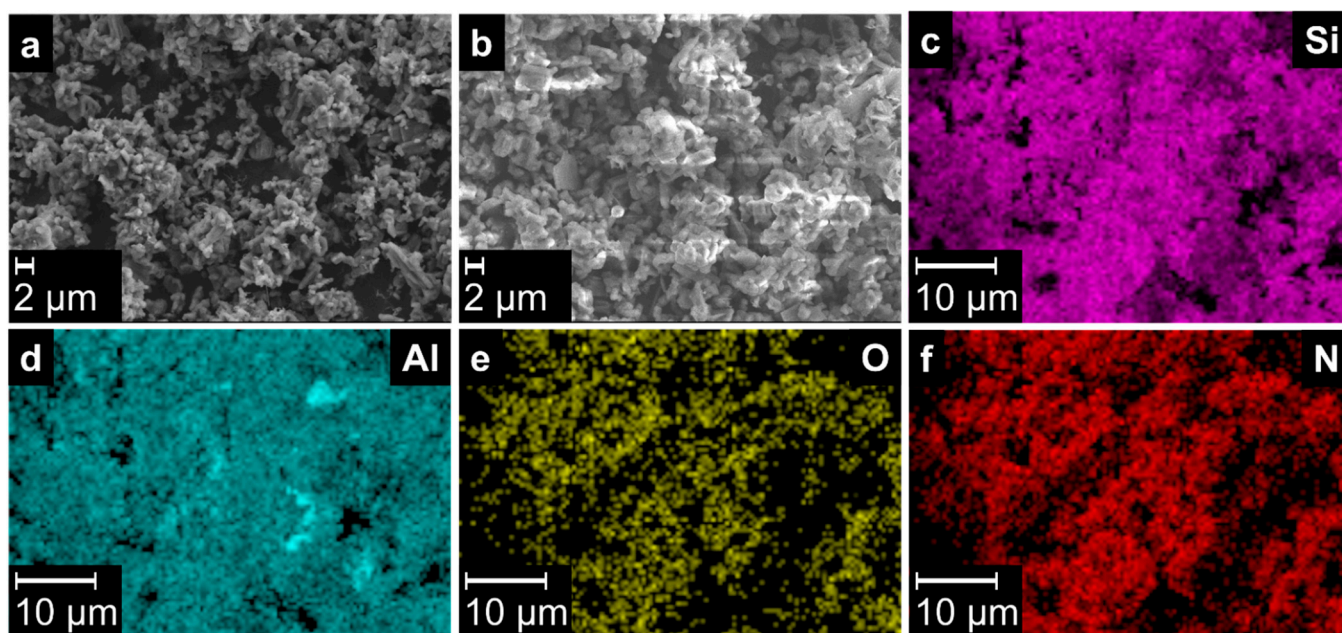


**Figure 2.** SEM-images of the samples SiAlON-1 (a) and SiAlON-2 (b) and element mapping with EDX spectroscopy for the sample SiAlON-1 (c–f).

## 2.2. Synthesis and Characterization of $\beta$ -SiAlON:NaF

The synthesis of  $\beta$ -SiAlON:NaF materials was carried out by high-temperature sintering of the mixtures of the corresponding  $\beta$ -SiAlONs with sodium fluoride NaF. The mixtures were preliminarily homogenized by vigorous grinding in an agate mortar with acetone followed by drying in air. The homogenized mixtures were pressed and pre-fired at 900 °C in air for 2 h and then under a stream of nitrogen (1 bar) at 1650 °C. The temperature was raised at a rate of  $\sim 400$  °C/h and kept for 2 h. Then, the mixtures were allowed to cool down naturally ( $\sim 12$  h). The samples after sintering appeared as gray pills. At the same time, some transparent crystalline whiskers formed on the walls of the crucibles. X-ray diffraction analysis showed that the whiskers consisted of two aluminum nitride polytypes. One of them was a typical hexagonal wurtzite-like AlN and the other one was identified as a tetrahedral zinc blende-like AlN, which is in fact metastable (Figure 3) [38]. Belonging to different structural types, both phases could be easily identified. The wurtzite-like AlN showed a set of peaks at 33.26, 35.96, 37.96, 49.80, 59.44, 65.98, 69.82, 71.64, 72.70, and 76.98 (ICDD 01-076-0702) and the zinc blende-like AlN showed peaks at 35.66, 41.38, 59.98, 71.46, and 76.30 (ICDD 01-080-0010).

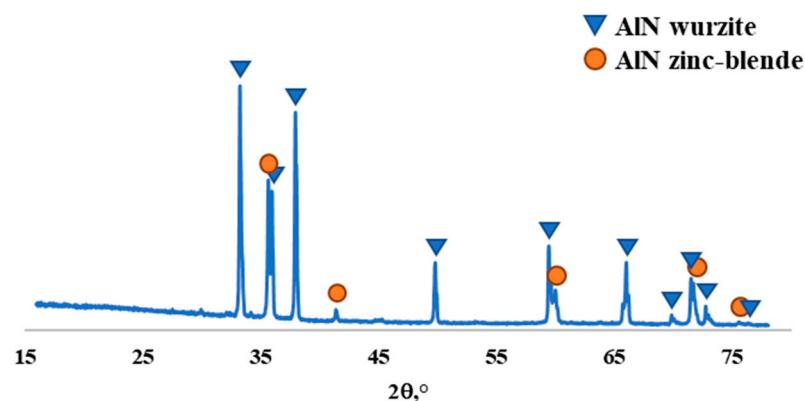
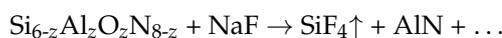


**Figure 3.** XRD-pattern of crystalline whiskers formed on the wall of the crucible after the sintering of SiAlON-2:0.5%NaF sample.

AlN most likely formed because of the partial decomposition of SiAlONs with the removal of silicon in the form of corresponding fluoride:



Silicon is well-known to form fluoride  $\text{SiF}_4$  easily, and that is the reason to use fluorides of alkali and alkali earth metals for the doping of SiAlONs with  $\text{Li}^+$ ,  $\text{Na}^+$ ,  $\text{Mg}^{2+}$ , etc., ions [26–29]. When the mentioned fluorides were used for doping, an excess of silicon was incorporated into the synthetic mixtures considering partial removing in the form of  $\text{SiF}_4$ . For  $\beta$ -SiAlONs it has also been found that interaction with fluorides at high temperatures (NaF-AlF<sub>3</sub> melt) led to the formation of  $\text{SiF}_4$ ,  $\text{Al}_2\text{O}_3$ , and  $\text{N}_2$  [34,37]. Since there was a lack of oxygen in the studied systems and the process occurred in a nitrogen atmosphere, the excess of aluminum formed after the decomposition of SiAlONs could form aluminum nitride. On the other hand, the phase composition and total element composition of the samples **SiAlON-1** and **SiAlON-2** after the sintering clearly point out that the decomposition according to the given scheme is not the only reaction pathway during the high-temperature interaction of SiAlONs with sodium fluoride NaF.

The sintered samples showed a complicate phase composition, which depended on the initial SiAlON structure and sodium fluoride loading. Thus, for the samples **SiAlON-1:NaF**,  $\text{Si}_5\text{AlON}_7$  was still a major phase after sintering. The sample **SiAlON-1:0.5%NaF** contained  $\text{Si}_2\text{Al}_4\text{O}_4\text{N}_6$  as a minor phase and in the sample **SiAlON-1:2.0%NaF** both  $\text{Si}_2\text{Al}_4\text{O}_4\text{N}_6$  and  $\text{Si}_{3.1}\text{Al}_{2.9}\text{O}_{2.9}\text{N}_{5.1}$  were present as minor phases with an almost equal content (Figure 4a,b, Table 2). On the contrary, for the samples **SiAlON-2:NaF**, the initial  $\text{Si}_2\text{Al}_4\text{O}_4\text{N}_6$  phase was not identified after sintering. The sample **SiAlON-2:0.5%NaF** contained  $\text{Si}_5\text{AlON}_7$  as a major phase and  $\text{Si}_{3.1}\text{Al}_{2.9}\text{O}_{2.9}\text{N}_{5.1}$  prevailed in the sample **SiAlON-2:2.0%NaF**. The minor phases in the sample **SiAlON-2:0.5%NaF** were  $\text{Si}_3\text{Al}_3\text{O}_3\text{N}_5$  and  $\text{Si}_{3.1}\text{Al}_{2.9}\text{O}_{2.9}\text{N}_{5.1}$  (Figure 4c, Table 2). Finally,  $\text{Si}_5\text{AlON}_7$  and  $\text{Si}_3\text{Al}_3\text{O}_3\text{N}_5$  could be considered as minor phases in the sample **SiAlON-2:2.0%NaF**, but all three phases in the sample were present in comparable amounts (Figure 4d, Table 2).

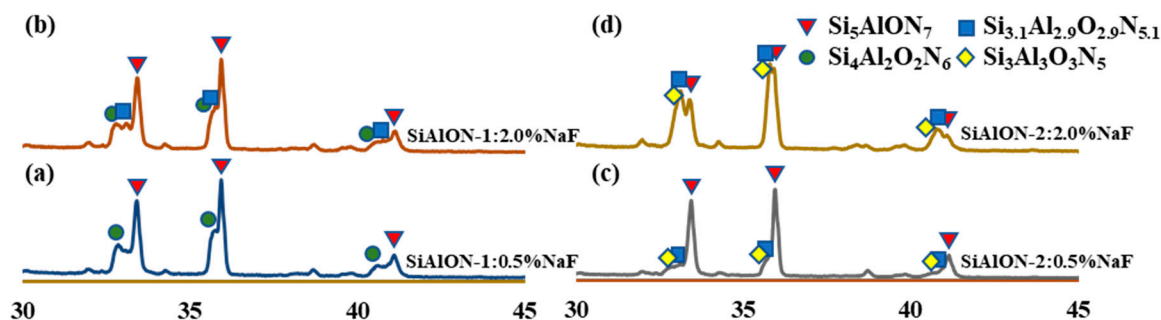


**Figure 4.** Characteristic parts of XRD patterns of the SiAlON:NaF samples after sintering: (a) SiAlON-1:0.5%NaF; (b) SiAlON-1:2.0%NaF; (c) SiAlON-2:0.5%NaF; (d) SiAlON-2:2.0%NaF (the full XRD patterns can be found in the Supplementary Materials).

**Table 2.** Phase composition of the SiAlON:NaF samples after sintering.

Sample	Major Phase	Minor Phases
SiAlON-1:0.5%NaF	$\text{Si}_5\text{AlON}_7$	$\text{Si}_4\text{Al}_2\text{O}_2\text{N}_6$
SiAlON-1:2.0%NaF	$\text{Si}_5\text{AlON}_7$	$\text{Si}_4\text{Al}_2\text{O}_2\text{N}_6$ and $\text{Si}_{3.1}\text{Al}_{2.9}\text{O}_{2.9}\text{N}_{5.1}$
SiAlON-2:0.5%NaF	$\text{Si}_5\text{AlON}_7$	$\text{Si}_3\text{Al}_3\text{O}_3\text{N}_5$ and $\text{Si}_{3.1}\text{Al}_{2.9}\text{O}_{2.9}\text{N}_{5.1}$
SiAlON-2:2.0%NaF	$\text{Si}_{3.1}\text{Al}_{2.9}\text{O}_{2.9}\text{N}_{5.1}$	$\text{Si}_5\text{AlON}_7$ and $\text{Si}_3\text{Al}_3\text{O}_3\text{N}_5$

Thus, the sintering of  $\beta$ -SiAlON with the addition of sodium fluoride NaF up to 2.0 wt.% led to the formation of phases with a higher aluminum content compared to the initial phases. The effect was more pronounced when the content of NaF was higher. At

the same time, the content of the phases enriched with aluminum was significantly higher than was expected assuming that silicon was removed in the form of  $\text{SiF}_4$  only. So, some other volatile silicon compounds formed at  $1650\text{ }^\circ\text{C}$ , which is consistent with the results of earlier studies [39]. On the other hand, for the **SiAlON-2** samples ( $\text{Si}_4\text{Al}_2\text{O}_2\text{N}_6$ ) a kind of disproportionation of the  $\text{Si}_4\text{Al}_2\text{O}_2\text{N}_6$  into  $\text{Si}_5\text{AlON}_7$  and  $\text{Si}_3\text{Al}_3\text{O}_3\text{N}_5$  (as well as to the closely related  $\text{Si}_{3.1}\text{Al}_{2.9}\text{O}_{2.9}\text{N}_{5.1}$ ) was observed after sintering. A similar phenomenon, i.e., the formation of SiAlONs with a higher aluminum content compared to the initial mixture, was found earlier when studying the formation of  $\beta$ -SiAlONs from the mixtures of  $\text{Si}_3\text{N}_4$ , AlN, and  $\text{Al}_2\text{O}_3$  with  $z$  values varying from 1 to 4 in a temperature range from  $1550$  to  $1750\text{ }^\circ\text{C}$  [40].

SEM images of the sintered samples showed the consolidation of individual crystallites into a compact material (Figure 5), however, the process was not completed, since individual crystallites were still possible to identify in the images, and a significant number of cavities were also observed. Structural densification was estimated from the change in density measured by hydrostatic weighing (Table 3). The theoretical densities for  $\beta$ -SiAlONs are  $3.160$  ( $z = 1$ ),  $3.118$  ( $z = 2$ ), and  $3.077\text{ g}\cdot\text{cm}^{-3}$  ( $z = 3$ ) [24], so the densities of the starting materials were below the theoretical values by  $\sim 3.8\%$  (**SiAlON-1**) and  $3.5\%$  (**SiAlON-2**). The initial density of **SiAlON-1** was  $3.08\text{ g}\cdot\text{cm}^{-3}$  and increased to  $3.15\text{ g}\cdot\text{cm}^{-3}$  after sintering with  $2.0\text{ wt.}\%$  of NaF, although phases with higher  $z$  values  $\text{Si}_4\text{Al}_2\text{O}_2\text{N}_6$  and  $\text{Si}_{3.1}\text{Al}_{2.9}\text{O}_{2.9}\text{N}_{5.1}$  formed (Table 2). The same trend was observed for the **SiAlON-2** materials. For **SiAlON-2**, an even sharper increase in density was observed after sintering with  $0.5\text{ wt.}\%$  of NaF. No doubt that was a result of the formation of  $\text{Si}_5\text{AlON}_7$  as a major phase and structural densification. When  $2.0\text{ wt.}\%$  of NaF was added, the density increased just a little bit because the structural densification was counterbalanced by the formation of less dense phases ( $\text{Si}_{3.1}\text{Al}_{2.9}\text{O}_{2.9}\text{N}_{5.1}$  and  $\text{Si}_3\text{Al}_3\text{O}_3\text{N}_5$ , see Table 2).

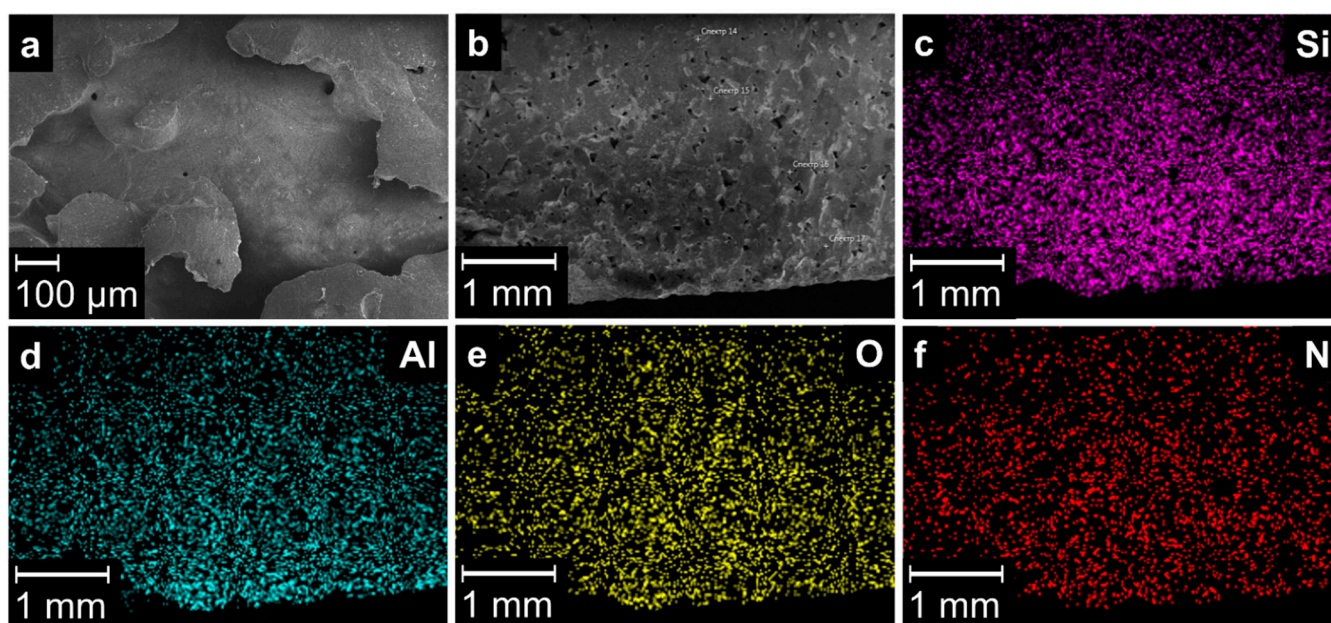


**Figure 5.** SEM images of the sample **SiAlON-2:2.0%NaF** (a,b) and element mapping with EDX spectroscopy (c–f).

Elemental analysis with EDX spectroscopy (including element mapping) showed just traces of sodium and fluorine in the composition of the material, so their contents could not be quantified. For all the major elements (Si, Al, O, and N), a uniform distribution in the samples volume was observed. The Si/Al ratio determined from the data of the EDX spectroscopy generally demonstrated a decrease with an increase in the content of NaF in the sintered sample (Table 3). That is in good agreement with the results of the

XRD analysis, indicating in most cases the formation of phases of  $\beta$ -SiAlONs with higher  $z$  values (except the SiAlON-2:0.5%NaF sample) (see Table 2).

**Table 3.** Average content of elements in the studied materials according to EDX spectroscopy and their densities measured by hydrostatic weighing.

Sample	Si, at. %	Al, at. %	O, at. %	N, at. %	Si/Al	Density, g/cm <sup>3</sup>
SiAlON-1	35.1	5.6	9.5	49.8	6.3	3.04
SiAlON-1:0.5%NaF	17.9	6.5	28.7	47.0	2.8	3.10
SiAlON-1:2.0%NaF	21.4	10.6	24.3	43.7	2.0	3.15
SiAlON-2	30.6	14.7	20.4	34.3	2.1	3.01
SiAlON-2:0.5%NaF	28.3	10.0	14.7	46.9	2.8	3.11
SiAlON-2:2.0%NaF	15.9	8.3	37.1	38.8	1.9	3.13

So, both the XRD and SEM/EDX data confirmed the formation of  $\beta$ -SiAlONs with lower Si/Al ratios (i.e., a higher  $z$  value) in the sintered samples compared to the starting materials. Many mechanical and physical properties of  $\beta$ -SiAlONs are known to be affected by  $z$  value, e.g., hardness, toughness, bending strength, thermal diffusivity, heat capacity, and thermal conductivity [24,41,42]. Mainly, an increase in  $z$  has a rather negative impact on the mechanical properties (Figure 6). However, if thermal conductivity is considered, it decreased with an increase in the  $z$  value, which is good when thermal insulative capability is in focus. In addition, an important point is that full-density ceramics are usually higher in the properties listed above, and the addition of fluorides is helpful for structural densification of  $\beta$ -SiAlONs. It is quite interesting that for the SiAlON-2:0.5%NaF sample formation, almost a single phase of Si<sub>5</sub>AlON<sub>7</sub> was observed with a noticeably higher density compared to the initial Si<sub>5</sub>AlON<sub>7</sub> (3.11 g·cm<sup>-3</sup> vs. 3.04 g·cm<sup>-3</sup>). That indicates a possible practical pathway not only for the transformation of different types of  $\beta$ -SiAlON into each other but also for the preparation of high-density ceramics by pressureless sintering at relatively low temperatures (compared to the traditionally used range of 1700–1850 °C) and without the incorporation of large amounts of fluorine. The latter is rather important if the material is used as a refractory, because, by decreasing the glass transition temperature and melting temperature, fluorine may have a negative impact on the high-temperature refractory performance [33].

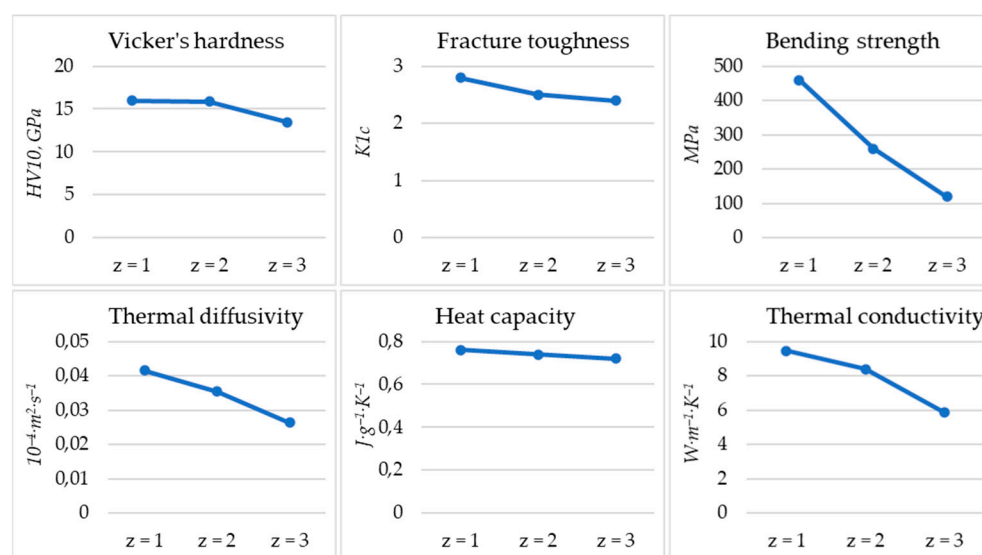


**Figure 6.** Mechanical and physical properties of  $\beta$ -SiAlONs depending on the  $z$  value (according to literature data [24,40,41]).

### 3. Materials and Methods

#### 3.1. Materials

The used starting materials were  $\beta$ -SiAlONs received from “Plasmotherm” LLC. According to the powder XRD analysis, the materials were almost monophase  $\text{Si}_5\text{AlON}_7$  (**SiAlON-1**) and  $\text{Si}_4\text{Al}_2\text{O}_2\text{N}_6$  (**SiAlON-2**) containing less than 3 v/v % of X-SiAlON  $\text{Si}_2\text{Al}_3\text{O}_7\text{N}$ . Sodium fluoride NaF (chemical grade) and acetone (chemical grade) were also used as received.

#### 3.2. Preparation of SiAlON:NaF

$\beta$ -SiAlON **SiAlON-1** or **SiAlON-2** was mixed with the corresponding amount of sodium fluoride NaF (0.5 or 2.0 wt.%). The mixture was homogenized through vigorous grinding in an agate mortar with acetone for 10 min followed by drying at 120 °C for 30 min in air. The homogenized mixture was pressed and pre-fired at 900 °C for 2 h in air and then sintered at 1650 °C for 2 h under a stream of nitrogen at 1 bar. The heating rate was ~400 °C/h, and after the sintering the samples were left to cool down to room temperature, which usually took ~12 h.

#### 3.3. Phase Composition

Phase composition of the starting materials and sintered **SiAlON:NaF** samples were determined by powder X-ray diffraction analysis. Powder XRD patterns of the samples at room temperature were collected on an Ultima IV diffractometer using  $\text{CuK}\alpha$  radiation ( $\lambda = 1.540598\text{\AA}$ ).

#### 3.4. Micro Images and Elemental Composition

Scanning electron microscopy images were taken with a scanning electron microscope Carl Zeiss Sigma VP using 10 kV accelerating voltage. The microscope was equipped with an energy dispersive X-ray spectroscopy detector, allowing for the determination of the elemental composition in a particular point as well as the elemental mapping in the defined area.

#### 3.5. Density Measurement

The density of the samples was measured by classical hydrostatic weighing. The samples were dry weighed ( $m_{dry}$ ) and then boiled in water for 40 min and weighed under water ( $m_{uw}$ ). Finally, the wet samples were weighed again in air ( $m_{wet}$ ). The density was calculated according to the formula:

$$\rho = \frac{m_{dry}}{m_{wet} - m_{uw}}$$

### 4. Conclusions

The interaction of  $\beta$ -SiAlONs  $\text{Si}_5\text{AlON}_7$  and  $\text{Si}_4\text{Al}_2\text{O}_2\text{N}_6$  with sodium fluoride NaF as a sintering additive at a temperature of 1650 °C in a nitrogen atmosphere was studied. It was found that the sintering resulted in the formation of free aluminum nitride, the partial removal of silicon and the formation of several phases also related to  $\beta$ -SiAlONs, whilst showing a lower Si/Al ratio compared to the starting materials. In the case of  $\text{Si}_5\text{AlON}_7$ ,  $\text{Si}_4\text{Al}_2\text{O}_2\text{N}_6$  and  $\text{Si}_{3.1}\text{Al}_{2.9}\text{O}_{2.9}\text{N}_{5.1}$  phases formed, however, the initial phase remained the major phase when both 0.5 and 2.0 wt.% of NaF was added. In the case of  $\text{Si}_4\text{Al}_2\text{O}_2\text{N}_6$ ,  $\text{Si}_3\text{Al}_3\text{O}_3\text{N}_5$  and  $\text{Si}_{3.1}\text{Al}_{2.9}\text{O}_{2.9}\text{N}_{5.1}$  phases formed together with the  $\text{Si}_5\text{AlON}_7$  phase, so a kind of disproportionation of the  $\text{Si}_4\text{Al}_2\text{O}_2\text{N}_6$  phase took place. When 0.5 wt.% of NaF was added to  $\text{Si}_4\text{Al}_2\text{O}_2\text{N}_6$ , the  $\text{Si}_5\text{AlON}_7$  phase was observed as a major phase, while the sintering of the sample with 2.0 wt.% NaF resulted in a material with a predominance of the  $\text{Si}_{3.1}\text{Al}_{2.9}\text{O}_{2.9}\text{N}_{5.1}$  phase, although the  $\text{Si}_5\text{AlON}_7$  phase content was still significant. The initial phase  $\text{Si}_4\text{Al}_2\text{O}_2\text{N}_6$  was not identified in both samples with 0.5 and 2.0 wt.% NaF after sintering. Figure 7 summarizes the changes in composition of  $\text{Si}_5\text{AlON}_7$  and  $\text{Si}_4\text{Al}_2\text{O}_2\text{N}_6$  under the high-temperature sintering with NaF under the nitrogen atmosphere. The SEM

images of all the samples showed that sintering in the presence of sodium fluoride lead to a significant reduction in the porosity of the materials, while the distribution of elements in the volume of the samples remained uniform, i.e., phase separation at the microlevel did not occur and the samples stayed homogeneous.

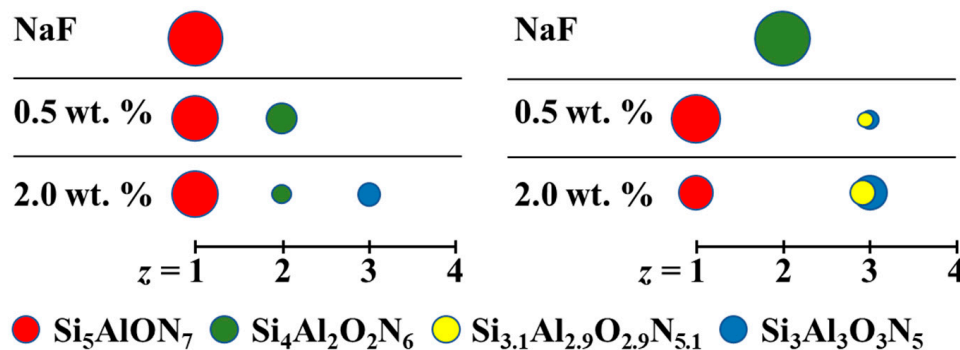


**Figure 7.** The changes in composition of  $\text{Si}_5\text{AlON}_7$  and  $\text{Si}_4\text{Al}_2\text{O}_2\text{N}_6$  under the high-temperature sintering with NaF.

To date, this is the first detailed study of the phase transformations occurring in  $\beta$ -SiAlONs in the presence of a small addition of alkali metal fluoride at high temperatures. In contrast to some previous studies, it dealt with the processes in the volume of the materials, not only on the surface [34,37]. The general revealed trend was a formation of phases with a lower Si/Al ratio (or higher  $z$  value). In parallel, structural densification also took place, which may counterbalance the decrease in mechanical properties, which usually happens when the  $z$  value increases. The sintered samples did not show a noticeable content of fluorine, so a lesser impact on the refractory properties may be expected in contrast to ceramics with high loading of fluorine [33]. Finally, the almost quantitative transformation of  $\text{Si}_4\text{Al}_2\text{O}_2\text{N}_6$  into  $\text{Si}_5\text{AlON}_5$  in the presence of 0.5 wt.% of NaF accompanied with densification by  $\sim 2\%$  seems to be perspective pathway to produce high-density ceramics from lower quality materials.

**Supplementary Materials:** The following supporting information can be downloaded at: <https://www.mdpi.com/article/10.3390/inorganics10090140/s1>. Figure S1. Powder X-ray Diffraction pattern of the sample **SiAlON-1:0.5%NaF**; Figure S2. Powder X-ray Diffraction pattern of the sample **SiAlON-1:2.0%NaF**; Figure S3. Powder X-ray Diffraction pattern of the sample **SiAlON-2:0.5%NaF**; Figure S4. Powder X-ray Diffraction pattern of the sample **SiAlON-2:2.0%NaF**; Figure S5. SEM images and elemental maps according to EDX spectroscopy data for the sample **SiAlON-1:0.5%NaF**; Figure S6. SEM images and elemental maps according to EDX spectroscopy data for the sample **SiAlON-1:2.0%NaF**; Figure S7. SEM images and elemental maps according to EDX spectroscopy data for the sample **SiAlON-2:0.5%NaF**; Figure S8. SEM images and elemental maps according to EDX spectroscopy data for the sample **SiAlON-2:2.0%NaF**.

**Author Contributions:** Investigation: N.S.A., V.P.S., N.A.O. and A.S.L.; writing—original draft preparation N.S.A.; writing—review and editing: N.S.A. and Y.F.K.; supervision—Y.F.K. All authors have read and agreed to the published version of the manuscript.

**Funding:** Financial support for this work was provided by the Russian Foundation on Basic Research—project #20-03-00455 “Ceramic materials based on sialons (oxonitridoaluminosilicates)”.

**Data Availability Statement:** Full data for all the samples including the XRD patterns, SEM images, and EDX spectra are available by request from the corresponding author.

**Acknowledgments:** Our special acknowledgements are to Ekaterina A. Obraztsova for the scanning electronic microscopy study of the samples.

**Conflicts of Interest:** The authors declare no conflict of interest.

## References

1. Kargin, Y.F.; Akhmadullina, N.S.; Solntsev, K.A. Ceramic materials and phosphors based on silicon nitride and sialon. *Inorg. Mater.* **2014**, *50*, 1325–1342. [[CrossRef](#)]
2. Akhmadullina, N.S.; Shishilov, O.N.; Kargin, Y.F. Sensitization effects in nitride materials doped with rare-earth metals ions. *Russ. Chem. Bull.* **2020**, *69*, 825–837. [[CrossRef](#)]
3. Yan, D.-S. Enhancing materials design capability through understanding multicomponent phase relationships. *Pure Appl. Chem.* **1998**, *70*, 509–515. [[CrossRef](#)]
4. Kurama, S.; Hermann, M.; Mandal, H. The effect of processing conditions, amount of additives and composition on the microstructures and mechanical properties of  $\alpha$ -SiAlON ceramics. *J. Eur. Ceram. Soc.* **2002**, *22*, 109–119. [[CrossRef](#)]
5. Thompson, D.P. Cooking up tougher ceramics. *Nature* **2002**, *417*, 237. [[CrossRef](#)]
6. Heimann, R.B. Silicon Nitride, a Close to Ideal Ceramic Material for Medical Application. *Ceramics* **2021**, *4*, 208–223. [[CrossRef](#)]
7. Shtansky, D.V.; Matveev, A.T.; Permyakova, E.S.; Leybo, D.V.; Konopatsky, A.S.; Sorokin, P.B. Recent Progress in Fabrication and Application of BN Nanostructures and BN-Based Nanohybrids. *Nanomaterials* **2022**, *12*, 2810. [[CrossRef](#)]
8. Jack, K.H. Sialons and related nitrogen ceramics. *J. Mater. Sci.* **1976**, *11*, 1135–1158. [[CrossRef](#)]
9. Gauckler, L.J.; Lukas, H.L.; Petzow, G. Contribution to the Phase Diagram  $\text{Si}_3\text{N}_4$ -AlN- $\text{Al}_2\text{O}_3$ - $\text{SiO}_2$ . *J. Am. Ceram. Soc.* **1975**, *58*, 346–347. [[CrossRef](#)]
10. Hampshire, S. *SiAlONs and the Representation of Phase Relationships. Encyclopedia of Materials: Technical Ceramics and Glasses, V. 2*; Elsevier: Amsterdam, The Netherlands, 2021; pp. 119–127. [[CrossRef](#)]
11. Xue, C.; Wang, D.; Zhang, J. Wear Mechanisms and Notch Formation of Whisker-Reinforced Alumina and Sialon Ceramic Tools during High-Speed Turning of Inconel 718. *Materials* **2022**, *15*, 3860. [[CrossRef](#)]
12. Metel, A.; Volosova, M.; Mustafaev, E.; Melnik, Y.; Seleznev, A.; Grigoriev, S. Plasma-Beam Processing of Tools Made of SiAlON Dielectric Ceramics to Increase Wear Resistance When Cutting Nickel–Chromium Alloys. *Coatings* **2022**, *12*, 469. [[CrossRef](#)]
13. Grigoriev, S.N.; Volosova, M.A.; Fedorov, S.V.; Okunkova, A.A.; Pivkin, P.M.; Peretyagin, P.Y.; Eshov, A. Development of DLC-Coated Solid SiAlON/TiN Ceramic End Mills for Nickel Alloy Machining: Problems and Prospects. *Coatings* **2021**, *11*, 532. [[CrossRef](#)]
14. Jack, K.H.; Wilson, W.I. Ceramics based on the Si-Al-O-N and Related Systems. *Nat. Phys. Sci.* **1972**, *238*, 28–29. [[CrossRef](#)]
15. Cao, G.Z.; Metselaar, R.  $\alpha'$ -Sialon Ceramics: A Review. *Chem. Mater.* **1991**, *3*, 242–252. [[CrossRef](#)]
16. Wang, H.; Chen, J.; Liu, Y.G.; Huang, Z.H.; Fang, M.H. In-Situ Synthesis of ( $O'$ + $\beta$ )-Sialon/Mullite Composite Materials from Coal Gangue. *Interceram-Int. Ceram. Rev.* **2015**, *64*, 112–115. [[CrossRef](#)]
17. Anya, C.C.; Hendry, A. Hardness, indentation fracture toughness and compositional formula of X-phase sialon. *J. Mater. Sci.* **1994**, *29*, 527–533. [[CrossRef](#)]
18. Thompson, D.P.; Korgul, P. Sialon X-phase. *Progr. Nitrogen Ceram.* **1983**, *321*, 375–380. [[CrossRef](#)]
19. Ekström, T.; Nygren, M. SiAlON Ceramics. *J. Am. Ceram. Soc.* **1992**, *75*, 259–276. [[CrossRef](#)]
20. Biswas, M.; Bandyopadhyay, S.; Sarkar, S. Sintering behavior & microstructure of SPS processed pure 15R-SiAlON polytype. *J. Alloys Compd.* **2018**, *768*, 130–135. [[CrossRef](#)]
21. Qin, H.; Li, Y.; Long, M.; Nie, X.; Jiang, P.; Xue, W. In situ synthesis mechanism of 15R-SiAlON reinforced  $\text{Al}_2\text{O}_3$  refractories by Fe-Si liquid phase sintering. *J. Am. Ceram. Soc.* **2018**, *101*, 1870–1879. [[CrossRef](#)]
22. Jack, K.H. The Fabrication of Dense Nitrogen Ceramics. *Mater. Sci. Res.* **1978**, *11*, 561–578. [[CrossRef](#)]
23. Oyama, Y.; Kamigaito, O. Solid Solubility of Some Oxides in  $\text{Si}_3\text{N}_4$ . *Jpn. J. Appl. Phys.* **1971**, *10*, 1637. [[CrossRef](#)]
24. Ekström, T.; Käll, P.O.; Nygren, M.; Olsson, P.O. Dense single-phase  $\beta$ -sialon ceramics by glass-encapsulated hot isostatic pressing. *J. Mater. Sci.* **1989**, *24*, 1853–1861. [[CrossRef](#)]
25. Hampshire, S. Silicon Nitride Ceramics. *Mater. Sci. Forum.* **2009**, *606*, 27–41. [[CrossRef](#)]
26. Sorrell, C.C. Silicon-nitride and related nitrogen ceramics. 1. Phase-equilibria and properties of reaction bonded and hot-pressed M-Si-O-N systems. *J. Aust. Ceram. Soc.* **1982**, *18*, 22–34.
27. Ziegler, G.; Heinrich, J.; Wötting, G. Relationships between processing, microstructure and properties of dense and reaction-bonded silicon nitride. *J. Mater. Sci.* **1987**, *22*, 3041–3086. [[CrossRef](#)]
28. White, G.V. New Synthesis Routes for SiAlON and SiAlON Ceramics. *Key Eng. Mater.* **2002**, *206*, 51–54. [[CrossRef](#)]
29. Junming, X.; Qian, L.; Linhua, G. Effect of LiF on Densification and Mechanical Properties of Dy- $\alpha$ -Sialon Ceramics. *J. Rare Earths* **2006**, *24*, 225–227. [[CrossRef](#)]
30. Ming, W.; Jiang, Z.; Luo, G.; Xu, Y.; He, W.; Xie, Z.; Shen, D.; Li, L. Progress in Transparent Nano-Ceramics and Their Potential Applications. *Nanomaterials* **2022**, *12*, 1491. [[CrossRef](#)]
31. Goldstein, A.; Krell, A. Transparent Ceramics at 50: Progress Made and Further Prospects. *J. Am. Ceram. Soc.* **2016**, *99*, 3173–3197. [[CrossRef](#)]
32. Qian, L.; Junming, X.; Wei, H. *Ceramic Materials and Components for Energy and Environmental Applications*; John Wiley & Sons: New York, NY, USA, 2010.
33. Hampshire, S.; Hanifi, A.R.; Genson, A.; Pomeroy, M.J. Ca-Si-Al-O-N Glasses: Effects of Fluorine on Glass Formation and Properties. *Key Eng. Mater.* **2007**, *352*, 165–172. [[CrossRef](#)]
34. Plachký, T.; Křest'an, J.; Korenko, M.; Medri, V.; Lenč'š, Z.; Šajgalík, P. Corrosion and oxidation behaviour of  $\beta$ -SiAlON ceramics via different processing route. *J. Ceram. Soc. Jpn.* **2009**, *117*, 482–488. [[CrossRef](#)]

35. Shimada, S.; Tanaka, M.; Kiyono, H.; MacKenzie, K.J.D. Microstructure and properties of various fluorine-containing SiAlON ceramics synthesized by HIPing. *J. Eur. Ceram. Soc.* **2001**, *21*, 2811–2819. [[CrossRef](#)]
36. Çalışkan, F.; Tatli, Z.; Genson, A.; Hampshire, S. Pressureless sintering of  $\beta$ -SiAlON ceramic compositions using fluorine and oxide additive system. *J. Eur. Ceram. Soc.* **2012**, *32*, 1337–1342. [[CrossRef](#)]
37. Plachký, T.; Křesťan, J.; Korenko, M.; Lenčes, Z.; Šajgalík, P. Corrosion of  $\beta$ -SiAlON in Molten Aluminium, Cryolite and NaCl-KCl Mixture. *Key Eng. Mater.* **2009**, *403*, 133–134. [[CrossRef](#)]
38. Yeh, C.; Lu, Z.W.; Froyen, S.; Zunger, A. Zinc-blende–wurtzite polytypism in semiconductors. *Phys. Rev. B Condens. Matter Mater. Phys.* **1992**, *46*, 10086–10097. [[CrossRef](#)]
39. Heuer, A.H.; Lou, V.L.K. Volatility Diagrams for Silica, Silicon Nitride, and Silicon Carbide and Their Application to High-Temperature Decomposition and Oxidation. *J. Am. Ceram. Soc.* **1990**, *73*, 2789–2803. [[CrossRef](#)]
40. Akhmadullina, N.S.; Lysenkov, A.S.; Konovalov, A.A.; Obraztsova, E.A.; Kim, K.A.; Kargin, Y.F. Synthesis and phases relationships of  $\text{Si}_{6-z}\text{Al}_z\text{O}_z\text{N}_{8-z}$  in a wide range of  $z$ . *Ceram. Int.* **2022**, *48*, 13348–13355. [[CrossRef](#)]
41. Kushan, S.R.; Uzun, I.; Dogan, B.; Mandal, H. Experimental and Finite Element Study of the Thermal Conductivity of  $\alpha$ -SiAlON Ceramics. *J. Am. Ceram. Soc.* **2007**, *90*, 3902–3907. [[CrossRef](#)]
42. Yi, X.; Zhang, W.; Akiyama, T. Thermal conductivity of  $\beta$ -SiAlONs prepared by a combination of combustion synthesis and spark plasma sintering. *Thermochim. Acta* **2014**, *576*, 56–59. [[CrossRef](#)]